ACS Energy LETTERS

http://pubs.acs.org/journal/aelccp

Upgrading Electrode/Electrolyte Interphases via Polyamide-Based Quasi-Solid Electrolyte for Long-Life Nickel-Rich Lithium Metal Batteries

Minjian Chen,[‖] Cheng Ma,[‖] Zhengping Ding, Liangjun Zhou, Libao Chen, Peng Gao, and Weifeng Wei*

Cite This: *ACS Energy Lett.* 2021, 6, 1280−1289

Read Online

ACCESS | Metrics & More | Article Recommendations | Supporting Information

ABSTRACT: Interface instability that stems from highly catalytic Ni-rich layered cathode and highly reactive lithium metal anode is the key to hindering the development of high-voltage lithium metal batteries (LMBs). Herein, we designed a multifunctional polyamide-based quasi-solid electrolyte (PAM-QSE) to construct a robust cathode electrolyte interphase (CEI) and stable solid electrolyte interphase (SEI) layers on both Ni-rich cathode and Li metal anode and improve flame-retardancy simultaneously. The SEI structure consists of rich lithiophilic N−$(C)_3$ to homogenize ion distribution and high ionic conductive Li_3N to guide the rapid transform of Li^+, effectively reshaping the uneven Li^+ plating/stripping behavior, whereas the CEI structure comprises high antioxidative amide organic species, which mitigates the detrimental parasitic reactions between active materials and electrolytes and alleviates surface structure degradation of cathode. As a result, $LiNi_{0.6}Co_{0.2}Mn_{0.2}O_2$/Li battery using flame-retardant PAM-QSE delivers excellent long-term cyclability even with high cathode loading (~6 mg cm^{-2}) and ultrathin Li (~50 μm).

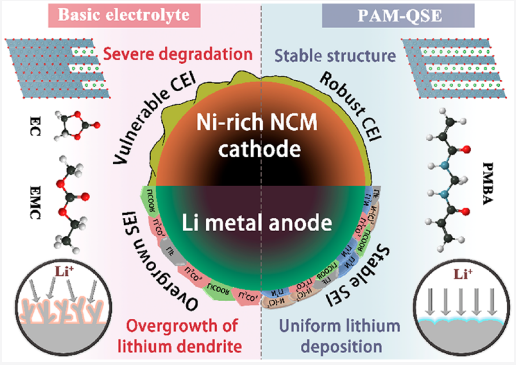

With the ever-increasing demand of high-energy storage technologies, traditional lithium-ion batteries (LIBs) are approaching to the theoretical energy density limit, which can no longer satisfy the application needs in diverse electronic devices and electric vehicles.[1−3] The combination of high-voltage, high-capacity nickel-rich layer $LiNi_xCo_yMn_{1-x-y}O_2$ (Ni-rich NCM, $x > 0.5$) cathode with Li metal anode that possesses an extremely high specific capacity (3860 mAh g^{-1}) and a low reduction potential (−3.04 V vs standard hydrogen electrode) has therefore been recognized as a promising way to raise the battery energy density up to 400 Wh kg^{-1}.[4−6] However, the practical application of high-voltage Li metal batteries (LMBs) is greatly hampered by the poor interfacial stability on both cathode and anode.[7−10] On one hand, the interphase constructed by commercial carbonate electrolytes has a low stability especially under the oxidation of Ni-rich NCM cathode, which results in inevitable accumulation of electrolytes oxidative decomposition products and irreversible surface degradation of cathode, leading to rapid capacity loss and voltage decay.[11−17] On the other hand, the high reactivity of Li metal anode promotes undesirable electrolyte consumption and uncontrollable Li dendrite growth, thus bringing about declined Coulombic efficiency and severe safety hazards.[18−22]

In order to tackle the above issues and maintain interfacial stability between electrodes and electrolyte during long-term cycling, considerable approaches have been explored.[23] Surface coating, considered as an artificial interface layer strategy, can substantially decrease the direct contact between electrodes and electrolytes.[24−28] For instance, Li et al. successfully coated $LiTaO_3$ on $LiNi_{1/3}Co_{1/3}Mn_{1/3}O_2$ by means of atomic layer deposition (ALD), and the coating layer effectively avoids the dissolution of cathode material in organic electrolytes.[29] Lang et al. demonstrated that a LiF layer on Li anode constructed via a solution coating method can minimize the side reactions with electrolyte and hinder the Li dendrite formation,[30]

Received: February 4, 2021
Accepted: March 12, 2021
Published: March 15, 2021

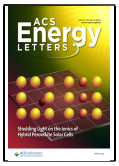

Scheme 1. Design Strategy of PAM-QSE: Schematic Illustration of the Interface Stabilization Mechanism for PAM-QSE

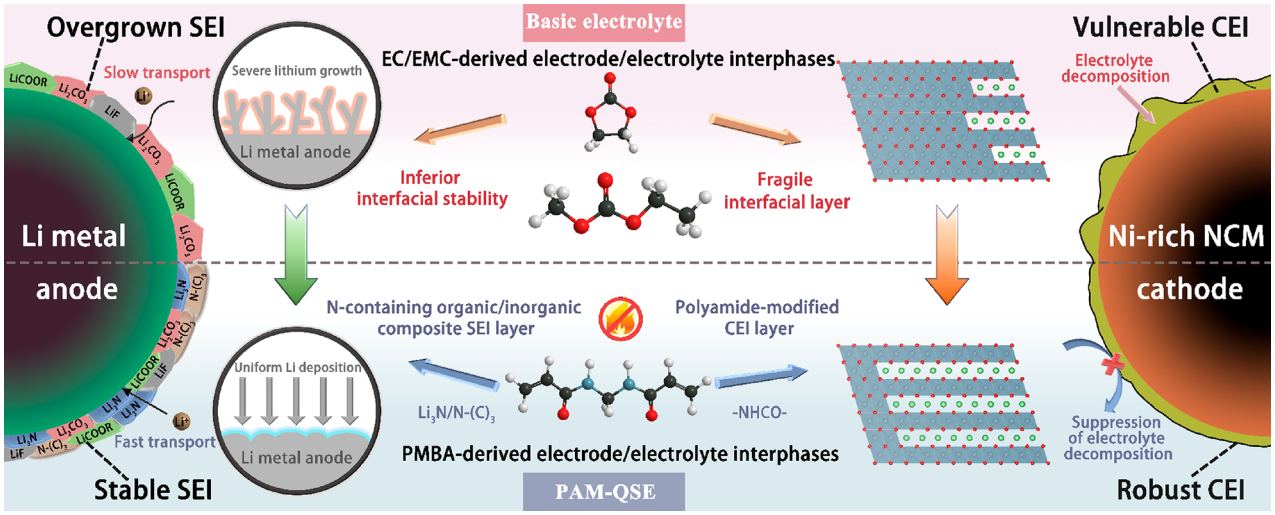

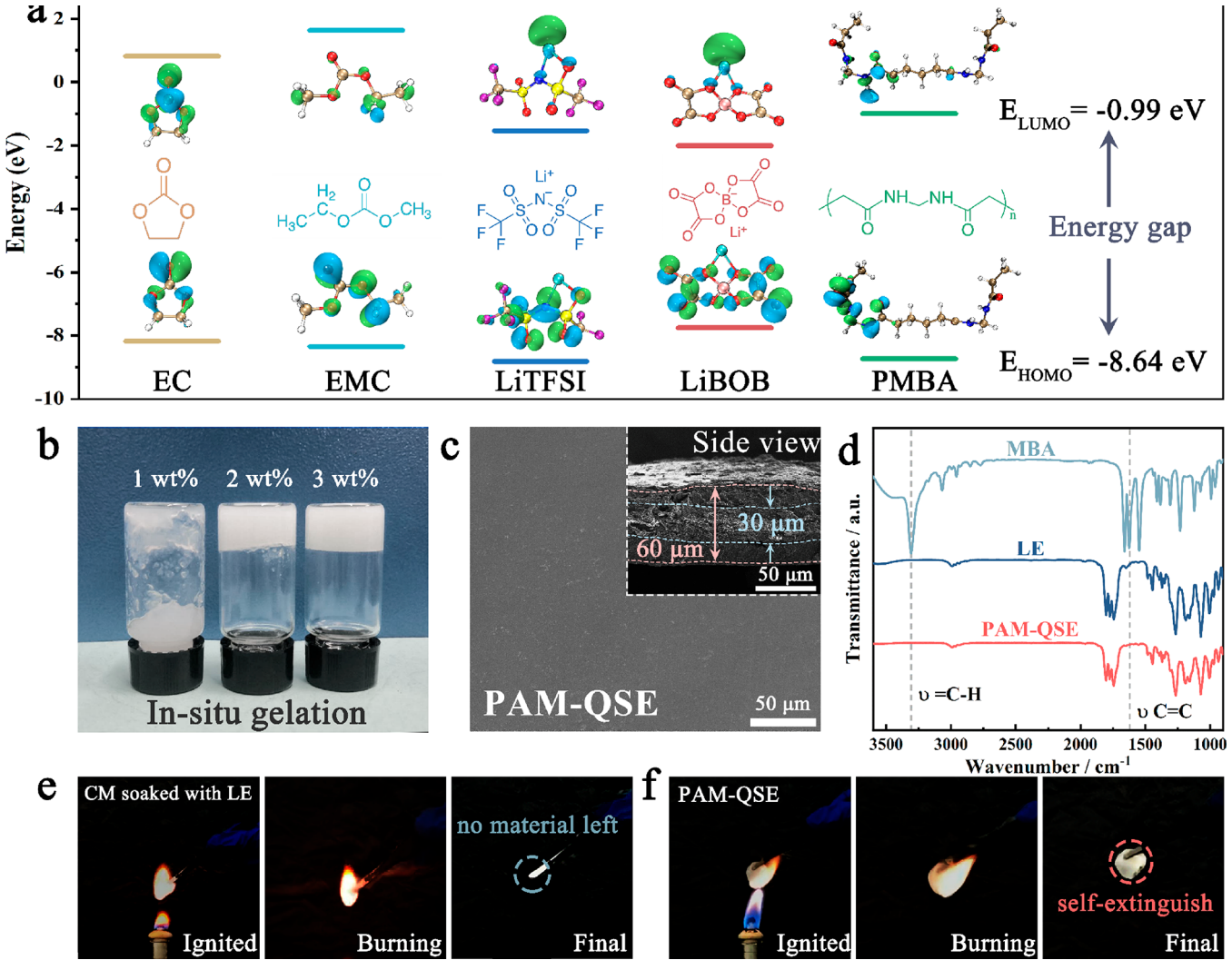

Figure 1. Molecular orbital energies, characterizations, and flame-retardant property of PAM-QSE: (a) calculated HOMO and LUMO energy levels of PMBA and electrolyte components; (b) optical photograph of PAM-QSE electrolyte with different weight fractions of PMBA; (c) scanning electron microscopy (SEM) images of PAM-QSE membrane; (d) FTIR spectra of the MBA, LE, and PAM-QSE; (e, f) specific burning test of cellulose membrane soaked with (e) LE and (f) PAM-QSE.

https://dx.doi.org/10.1021/acsenergylett.1c00265
ACS Energy Lett. 2021, 6, 1280−1289

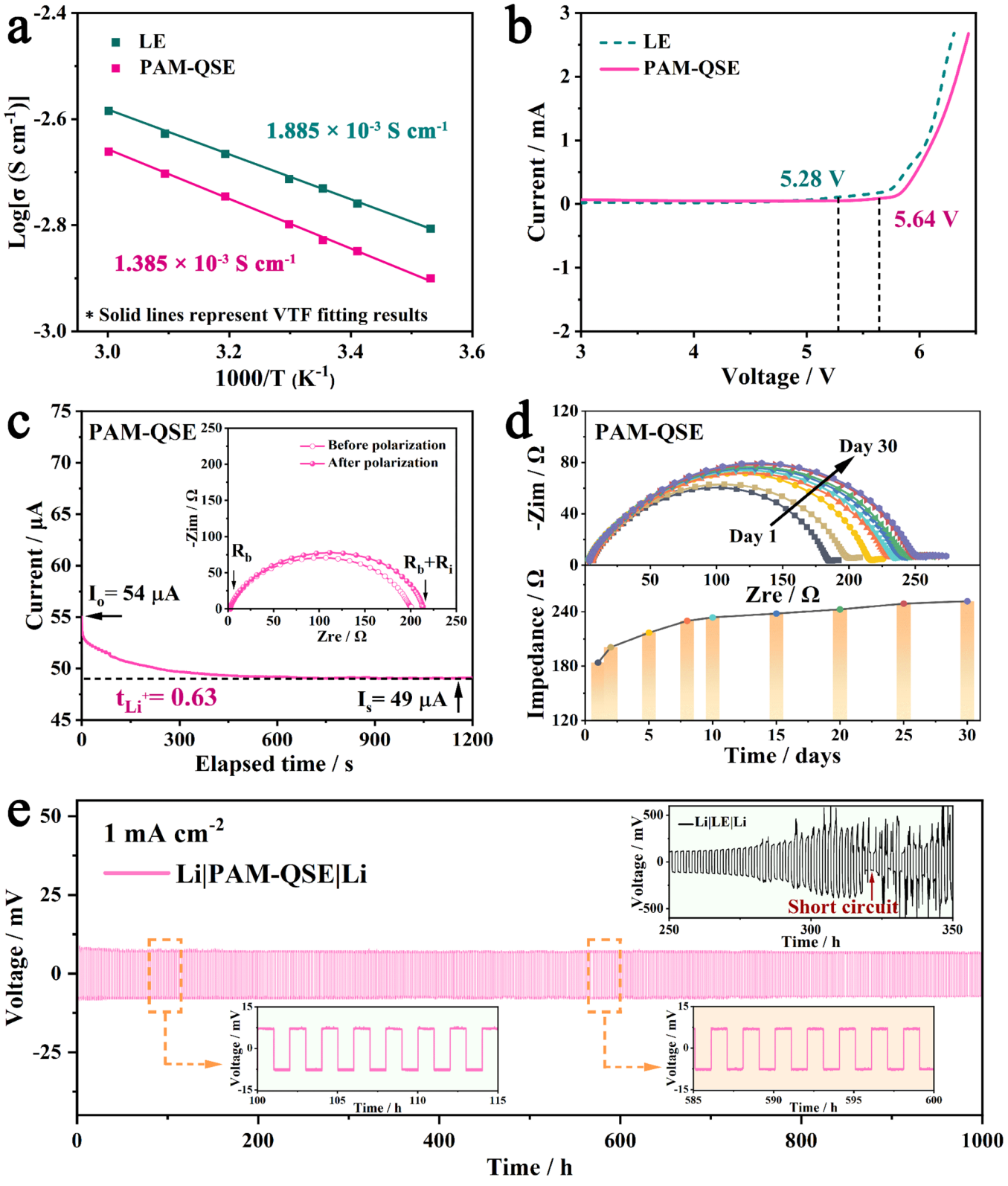

Figure 2. Electrochemical properties of PAM-QSE: (a) ionic conductivities of PAM-QSE at various temperatures; (b) linear sweep voltammograms of PAM-QSE at a scan rate of 5 mV s^{-1} using stainless steels as the working electrodes and Li foils as the counter and reference electrodes; (c) chronoamperometry profile of a symmetric Li/PAM-QSE/Li battery under a polarization potential of 5 mV and the corresponding Nyquist plots of electrochemical impedance spectroscopy before and after polarization (inset); (d) interfacial resistances of symmetric Li/PAM-QSE/Li battery with Nyquist plots (inset) at various aging times; (e) Li plating/stripping profiles of symmetric Li/Li batteries with PAM-QSE (red line) and the LE (black line shown in the inset) at a current density of 0.5 mA cm^{-2}.

whereas most coating layers are vulnerable to failure due to repetitive mechanical deformation during prolonged cycling and nonelectrochemically active coating layers will sacrifice the battery energy density.[23,31]

https://dx.doi.org/10.1021/acsenergylett.1c00265
ACS Energy Lett. 2021, 6, 1280−1289

Considering the electrolyte contacts with both cathode and anode, functional electrolyte additives are extensively utilized to regulate electrode/electrolyte interphases.[32−35] Liang et al. adopted lithium difluoro(oxalato)borate salt to in situ construct an amorphous cathode electrolyte interphase, resulting in preferable interfacial stability.[36] Sun et al. developed sodium bis(trifluoromethanesulfonyl)imide as a novel additive to provide electrostatic shielding and interfacial passivation effect for Li metal anode, boosting the high reversibility of Li metal batteries.[37] Nevertheless, most electrolyte additives could only optimize a single interphase layer on either cathode or anode, and electrolyte leakage and flammability aggravate the safety hazards of Ni-rich NCM/Li metal batteries.[38,39] Hence, it is of significant importance to develop a quasi-solid/solid electrolyte to stabilize both cathode electrolyte interphase (CEI) layer on Ni-rich cathode and solid electrolyte interphase (SEI) layer on Li anode and upgrade flame-retardancy concurrently.

In this work, we proposed a polyamide-based quasi-solid electrolyte (PAM-QSE) via in situ gelation with 3 wt % *N*,*N*′-methylenebisacrylamide (MBA) as cross-linker and interface reinforced component. Compared to the basic liquid electrolyte (LE), PAM-QSE delivers remarkable electrode/electrolyte interphase stability and flame-retardancy (Scheme 1): (1) A composite organic/inorganic SEI structure comprising abundant nitrides such as $N-(C)_3$ and Li_3N is spontaneously constructed on the surface of Li metal, in which lithiophilic $N-(C)_3$ guides the homogeneous Li^+ distribution and the Li_3N with high ionic conductivity inhibits the growth of lithium dendrite. (2) Durable CEI structure derived from high antioxidative amide organic groups could effectively isolate cathode materials from direct contact with electrolyte and thus suppresses interfacial parasitic reactions and structural degradation of Ni-rich NCM cathode. (3) Highly cross-linked structure of PMBA ensures a high electrolyte uptake with marginal ion-conduction loss and substantially improved flame-retardant property. This study could open up the possibilities for electrode/electrolyte interphases via functionalized quasi-solid electrolyte design and promote the development of practical high voltage LMBs with high energy density and high safety.

Synthesis and Characterization of PAM-QSE. Density functional theory (DFT) calculations were first utilized to estimate the oxidation and reduction activities of poly(*N*,*N*′-methylenebisacrylamide) (PMBA) and other electrolyte components according to their molecular orbital energy levels. As shown in Figure 1a and Table S1, PMBA exhibits a relatively lower lowest unoccupied molecular orbital (LUMO) than solvent molecules, making it more preferential to be reduced at Li anode interface, and hence dominates the formation of SEI layer with beneficial N-containing compounds as verified by previous studies.[40−43] Meanwhile, the highest occupied molecular orbital (HOMO) of PMBA is also lower than that of most solvents and lithium salts, demonstrating a high oxidation stability. It is expected to enclose the electrolyte inside the PMBA cross-linked structure and to protect them from continuous decomposition during high voltage operations. The effective regulation of electrochemical behavior on both high-voltage cathode and Li anode interfaces endows the PAM-QSE with great application potential in Ni-rich NCM/Li metal batteries.

The PAM-QSE was prepared via in situ thermal initiated radical polymerization (Figure S1) with MBA as cross-linking agent and porous cellulose membrane (CM) consisting of randomly arranged nanofibers as supporting framework (Figure S2). After heating at 60 °C for 4 h, the gelatinous electrolyte components (Figure 1b) evenly covered and infiltrated into the pores of cellulose membrane, and a dense quasi-solid polymer electrolyte membrane with the thickness of ∼60 μm was obtained (Figure 1c). To verify the polymerization of MBA monomer, Fourier transform infrared (FTIR) spectra were conducted (Figure 1d). Apparently, the absorption peaks at around 1626 and 3065 cm^{-1} that correspond to the vibrations of C═C and ═C−H, respectively, appear in the spectrum of MBA and disappear after thermal polymerization, demonstrating that the PAM-QSE was successfully synthesized.

Flammable liquid electrolyte (LE) is a major safety hazard associated with high-voltage LMBs. To demonstrate the flame-retardant property upon thermal initiation, combustion tests with LE and PAM-QSE are presented in Figure 1e,f. Upon exposure to direct flame, the cellulose membrane soaked with quantitative LE was ignited and burned out rapidly with no materials left. In contrast, PAM-QSE effectively shortened the burning time as well as inhibited the spread of flame and ultimately realized self-extinguishing after ignition. The underlying reason is that the amide polymer network could generate N-containing radicals and noncombustible ammonia/water gas to weaken or even terminate the transfers of heat, fuel, and oxygen.[44,45]

Electrochemical Tests of PAM-QSE. Figure 2a displays the temperature dependence of ionic conductivity of PAM-QSE in a temperature range from 10 to 60 °C. The PAM-QSE manifests a high ionic conductivity of 1.385×10^{-3} S cm^{-1} at 25 °C, approaching that of liquid electrolyte (1.885×10^{-3} S cm^{-1}), which can be attributed to the high electrolyte uptake (97 wt %) of the PMBA cross-linked network. Linear sweep voltammetry (LSV) measurements were performed to explore the electrochemical stability of electrolytes (Figure 2b and Figure S3). Notably, the introduction of antioxidant PMBA broadens the electrochemical oxidation decomposition potential to 5.64 V, when compared to 5.28 V for the basic liquid electrolyte. Such a high electrochemical window of PAM-QSE is sufficient to meet the requirement for high-voltage LMBs. Besides, the Li^+ transference number (t_{Li}^+) of the PAM-QSE reaches up to 0.63, greatly exceeding the value of liquid electrolyte (0.39) as shown in Figure 2c, Figure S4, and Table S2. The increased t_{Li}^+ benefits from the additional Li^+ migration channels provided by lithiophilic amide groups with high dielectric constant, which is favorable to reduce the nonuniform concentration gradient and improve the cycling stability of Li metal anode.[46−48]

To investigate the aging stability of PAM-QSE, Li/PAM-QSE/Li symmetrical battery was fabricated for alternating current (AC) impedance spectroscopy tests with storage times. As shown in Figure 2d, the interfacial resistance displays minor increase from 184 Ω to 229 Ω within 8 days and becomes steady in the subsequent time, indicative of outstanding interfacial compatibility between PAM-QSE and Li metal anode. Electrochemical detection of Li plating/stripping behavior on Li metal anode and the cycling stability was further performed by the galvanostatic charge/discharge voltage profiles in symmetric batteries with PAM-QSE and LE (Figure 2e). It is observed that PAM-QSE endows the symmetric battery with a small polarized potential and outstanding long-term cycling performance over 1000 h at 1

https://dx.doi.org/10.1021/acsenergylett.1c00265
ACS Energy Lett. 2021, 6, 1280−1289

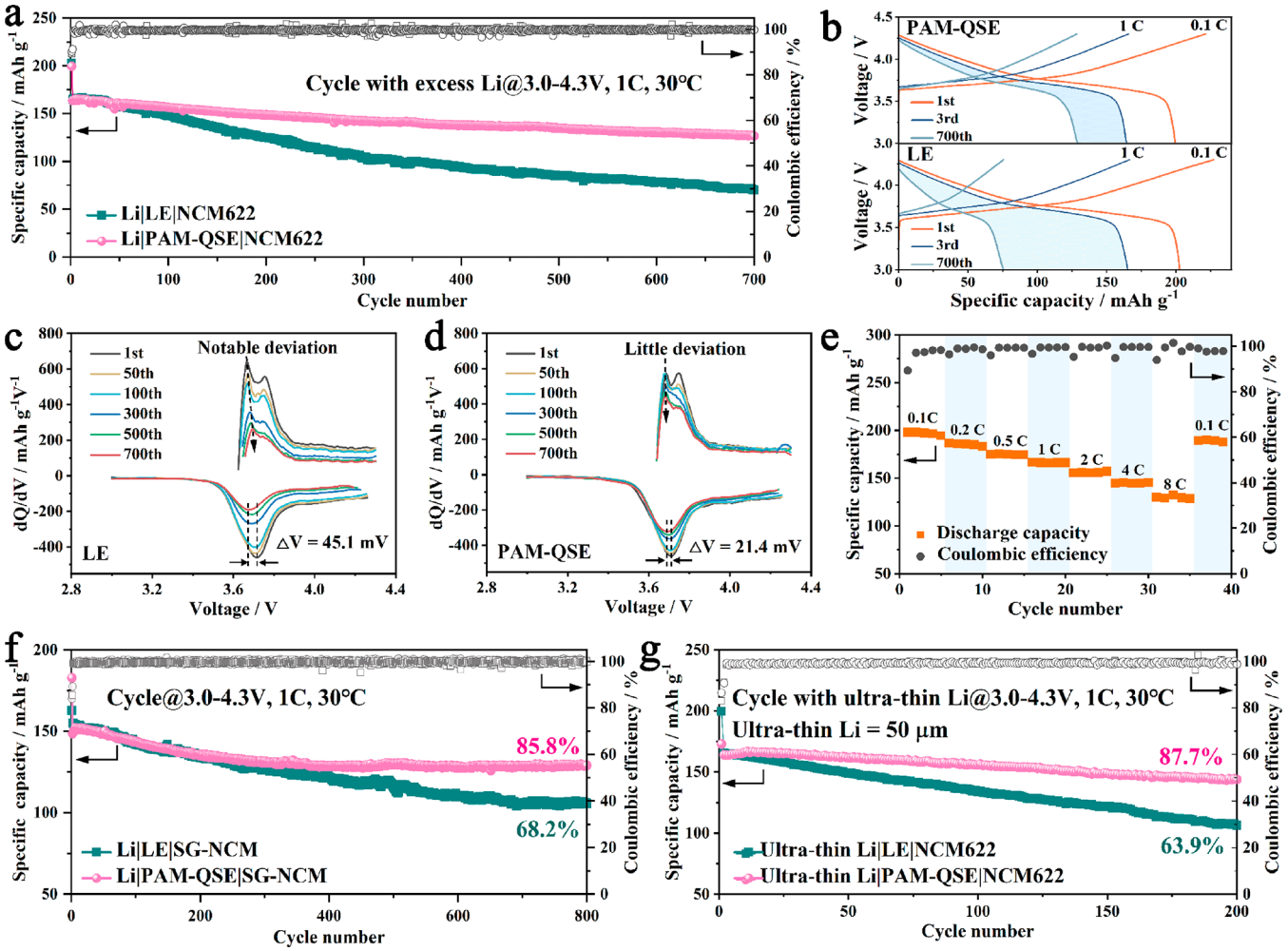

Figure 3. Electrochemical performance of Ni-Rich NCM/Li metal batteries: (a) cycling performance, (b) charge−discharge curves, and (c, d) dQ/dV profiles of polycrystalline NCM/excess Li metal batteries with LE and PAM-QSE at 1 C; (e) rate performance of the polycrystalline NCM/Li metal battery using PAM-QSE; (f) single-crystalline NCM/excess Li metal batteries at 1 C using LE and PAM-QSE; (g) cycling performance of polycrystalline NCM/ultrathin Li metal batteries at 1 C.

mA cm^{-2}, revealing a durable SEI layer and highly stable Li plating/stripping reversibility without the safety hazard from Li dendrites growth. On the contrary, the LE based symmetric battery presents a gradually increased polarized potential hysteresis due to the thick accumulated SEI layer and ultimately short circuit in 280 h caused by excessive dendritic Li piercing through the separator.[17] Additionally, the remarkable interfacial compatibility between PAM-QSE and Li metal is also validated by stable cycling performance at other current densities of 0.5 and 5 mA cm^{-2} (Figure S5) as well as the relatively steady interfacial resistance during cycling (Figure S6).

Electrochemical Performance of Ni-Rich NCM/Li Metal Batteries. The electrochemical performance of NCM ($LiNi_{0.6}Co_{0.2}Mn_{0.2}O_2$)/Li metal batteries was examined to evaluate the application feasibility of the PAM-QSE. Figure 3a presents the long-term cycling performance of polycrystalline NCM/excess Li metal batteries with limited electrolyte (30 μL) at 1 C (1 C = 160 mAh g^{-1}) in the voltage range of 3−4.3 V. The batteries with both LE and PAM-QSE exhibit almost the same charge/discharge voltage profiles and deliver a similar specific capacity (~199.6 mAh g^{-1}) in the initial cycle (Figure 3b). Differently, compared to the severe capacity degradation for LE based battery, the battery using PAM-QSE achieves a remarkable capacity retention of ~80% after 700 cycles with a high reversible capacity of 129.3 mAh g^{-1}, which is also superior to the other reported NCM/Li metal batteries in the literature (Table S3). To attain more insights into the improved cycling performance, the profiles of differential capacity versus the electrode potential (dQ/dV) derived from different charge−discharge curves are displayed in Figure 3c,d. Noticeably, the variation of reduction peaks of the battery with PAM-QSE exhibits a smaller potential increment of 21.4 mV than that of LE based battery (45.1 mV) over 700 cycles, implying that PAM-QSE is effective to mitigate the undesirable interface deterioration and reduce battery overpotentials during cycling. Additionally, due to the trivial loss of ionic conductivity in PAM-QSE, the NCM/PAM-QSE/Li battery can deliver specific discharge capacities of 198.5, 186.5, 175.2, 166.5, 155.7, 144.5, and 130.2 mAh g^{-1} at 0.1, 0.2, 0.5, 1, 2, 4, and 8 C, as shown in Figure 3e, indicating an excellent rate performance comparable to LE based battery (Figure S7 and Table S4).

Moreover, after replacement of polycrystalline $LiNi_{0.6}Co_{0.2}Mn_{0.2}O_2$ cathode with single-crystalline $LiNi_{0.6}Co_{0.2}Mn_{0.2}O_2$ cathode, the capacity retention of NCM/

https://dx.doi.org/10.1021/acsenergylett.1c00265
ACS Energy Lett. 2021, 6, 1280−1289

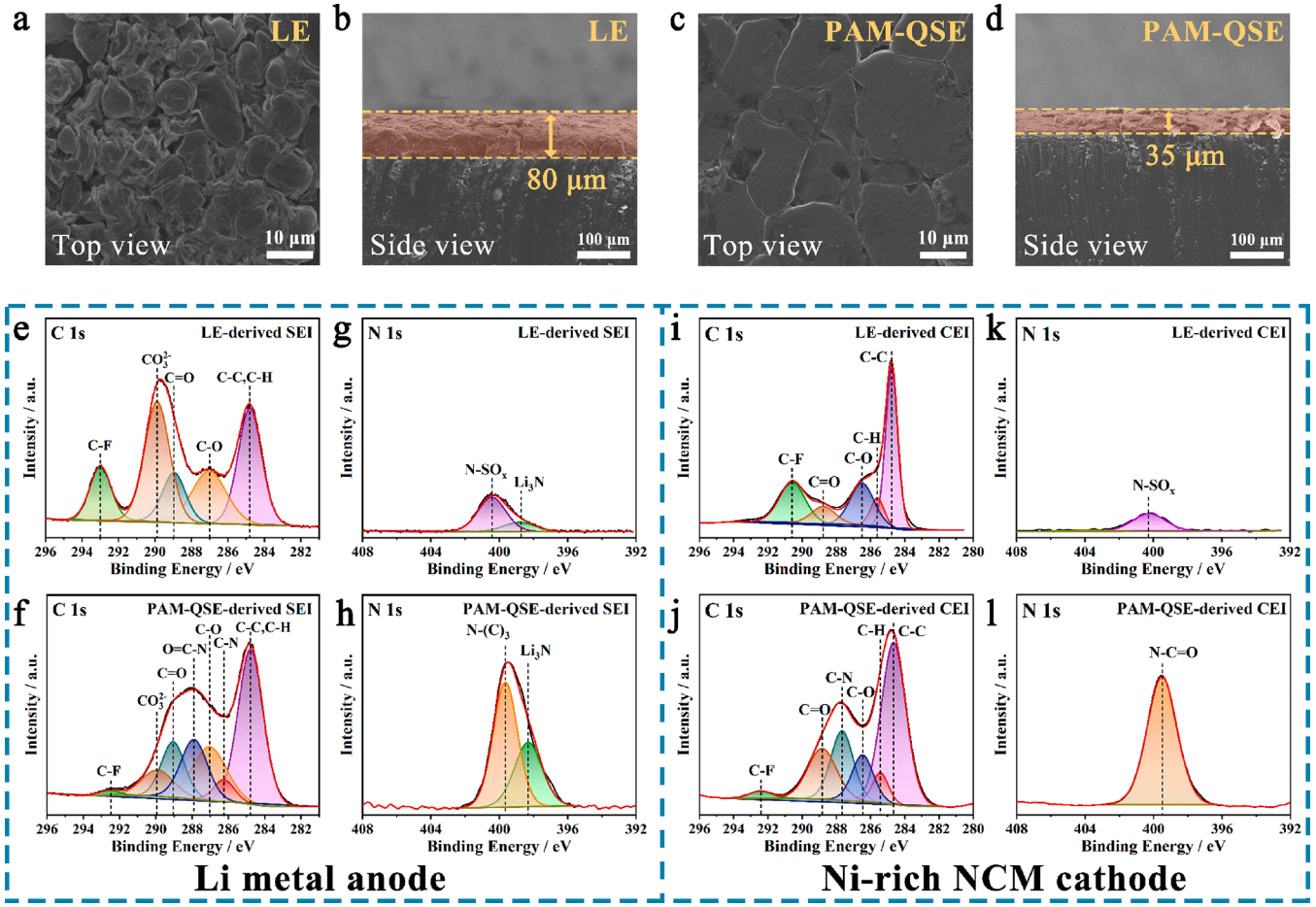

Figure 4. Surface characterizations of cycled Li anodes and NCM cathodes. SEM images of the cycled Li metal anodes with LE (a, b) and PAM-QSE (c, d) after 200 cycles. High resolution XPS spectra of C 1s (e, f) and N 1s (g, h) taken from cycled Li metal anodes with LE and PAM-QSE after 200cycles. XPS spectra of C 1s (i, j) and N 1s (k, l) taken from cycled NCM cathodes with LE and PQM-QSE after 200 cycles.

excess Li metal battery using PAM-QSE can further increase to 85.8% over 800 cycles (Figure 3f). In order to further verify the superiority of PAM-QSE, we investigated the cycle reversibility of polycrystalline NCM/ultrathin Li metal batteries using high loading $LiNi_{0.6}Co_{0.2}Mn_{0.2}O_2$ (~6 mg cm^{-2}) as cathode and Li deposited copper (Cu) electrodes as anode (~50 μm) (Figure 3g and Figure S8). Under practical conditions, the LE based battery failed rapidly within 200 cycles, and severe electrolyte side reactions accompanied by continuous consumption of active Li may account for the drastic capacity decay, whereas the cycle life of practical battery with PAM-QSE is extended significantly with a reversible discharge capacity of 143.8 mAh g^{-1} after 200 cycles, showing notable enhancement on cycling stability. This excellent electrochemical performance of NCM/PAM-QSE/Li metal battery makes it a promising high energy density battery system for large-scale energy storage applications.

Interface Structure and Chemistry of Cycled Li Metal Anodes and Ni-Rich NCM Cathodes. Considering that the evolution of interface structure and chemistry play a key role in battery performance, one question that is raised regarding the improved performance is how the PMBA additive could substantially change the interfaces structurally and chemically. SEM analysis was first carried out to investigate the surface morphology of the Li metal anodes after 200 cycles. The Li anode with LE presents small deposited particles mixed with needle-like dendrites (Figure 4a). This surface layer cannot shield the bulk Li against electrolyte attack, resulting in a thick Li corrosion layer of more than 80 μm (Figure 4b). In contrast, a smooth and compact surface with large and flat plate-like structures is observed on cycled Li anode with PAM-QSE, which can lessen the exposure of electrolyte toward the fresh Li metal and thus lead to a much thinner Li corrosion layer of 35 μm (Figure 4c,d).

The differences in the morphology of cycled Li metal anodes are closely correlated to the SEI layer structure, so X-ray photoelectron spectroscopy (XPS) analysis was carried out on the above Li anodes. Li anode with LE presents copious organic species caused by severe electrolyte decomposition, including C−C/C−H, C−O, C═O, CO_3, C−F, and N−SO_x (Figure 4e,g and Figure S9). Note that the content of above commonly decomposed products is obviously reduced on the Li anode with PAM-QSE (Figure 4f), and additional peaks at 286.4 eV (C−N) and 288.8 eV (O═C−N) in C 1s spectrum as well as at 398.5 eV (Li_3N) and 399.7 eV (N−$(C)_3$) in N 1s spectrum also appear (Figure 4h), indicating the participation of PMBA in the formation of organic/inorganic composite SEI layer.[49,50] It has been confirmed that lithiophilic N−$(C)_3$ can provide Lewis base sites to guide the uniform distribution of Li^+,[51] and Li_3N acts as an excellent Li-ion conductor to facilitate Li^+ transport to Li metal anode surface.[51−53] Thus, the stable and robust composite SEI layer containing

https://dx.doi.org/10.1021/acsenergylett.1c00265
ACS Energy Lett. 2021, 6, 1280−1289

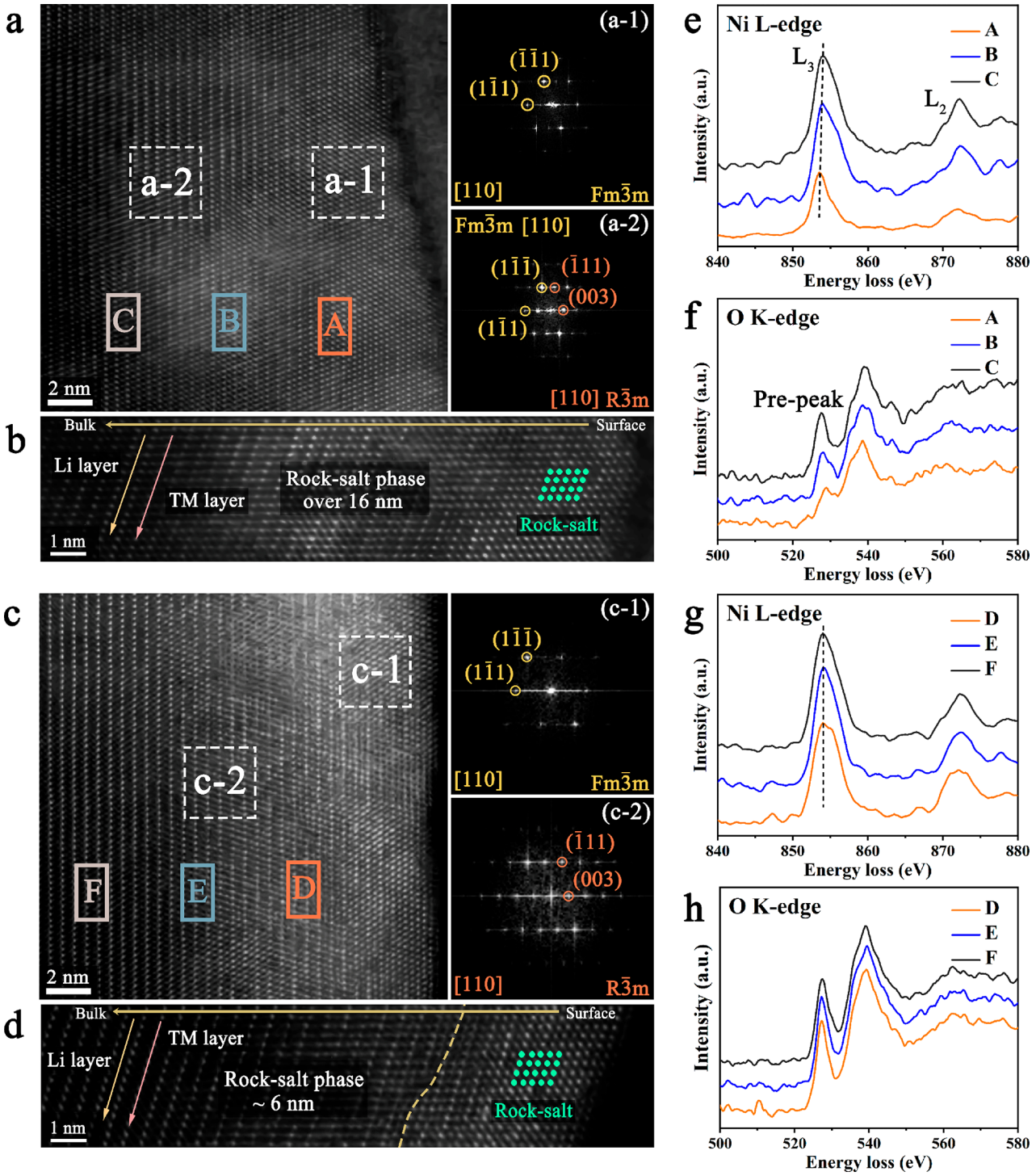

Figure 5. Quantification of surface degradation on cycled NCM cathodes. HAADF-STEM images and corresponding FFT patterns of the cycled NCM electrodes with (a) LE and (c) PAM-QSE after 200 cycles. Magnified HAADF-STEM images of the cycled NCM electrodes with (b) LE and (d) PAM-QSE. EELS spectra for the Ni L-edge and O K-edge from surface to interior of NCM electrodes cycled with (e, f) LE and (g, h) PAM-QSE.

synergistic N−$(C)_3$ and Li_3N not only suppresses the excessive decomposition of electrolyte but also promotes homogeneous Li^+ platting/stripping behavior.

XPS spectra of the cycled NCM cathodes were also collected and compared in Figure 4i−l and Figure S10. The low intensity of metal−O in O 1s spectrum and the high intensity of LiF in F 1s spectrum illustrate that the surface of NCM electrode cycled with LE was covered with more side reaction byproducts (Figure S10a,c), while the CEI layer with PAM-QSE contains rich antioxidative N−C═O, which greatly prevents the catalytic decomposition of electrolyte and suppresses surface degradation of active cathode materials (Figure 4l). Besides, electrochemical impedance spectroscopy (EIS) and cyclic voltammetry (CV) reveal an enhanced Li^+ diffusion coefficient and decreased interfacial resistance for PAM-QSE based battery (Figures S11 and S12 and Table S5),

https://dx.doi.org/10.1021/acsenergylett.1c00265
ACS Energy Lett. 2021, 6, 1280−1289

suggesting that the generated CEI with PAM-QSE is thinner and more durable.

More evidence of surface protection for NCM cathode by PAM-QSE can be obtained from atomic-resolution scanning transmission electron microscopy (STEM) and electron energy loss spectroscopy (EELS) characterizations. According to high-angle annular dark-field (HAADF) STEM images and corresponding fast Fourier transform (FFT) patterns, the cycled NCM cathode with LE experiences severe irreversible phase transformation from well-ordered layered phase to the electrochemically inactive rock-salt phase with a thickness of about 16 nm (Figures 5a,b and S13a). Remarkably, this detrimental surface reconstruction is effectively suppressed by PAM-QSE, showing only a few nanometes thick rock-salt phase on the cathode surface after 200 cycles (Figures 5c,d and S13b), which implies that PAM-QSE plays a key role to stabilize surface chemistry and structure of NCM cathode during extended cycling.

EELS line scanning was performed to further elucidate the local chemistry evolution from surface to interior of the cycled NCM with LE and PAM-QSE (Figure 5e–h). Ni $L_{2,3}$-edge of NCM electrode cycled with LE presents noticeable leftward energy shifts accompanied by a slight increase of the intensity ratio of L_3 and L_2 (Table S6), demonstrating a higher Ni^{2+} concentration on the external surface.[54] Moreover, the O K-edge prepeak becomes weaker as well as shifts to a higher energy, indicative of the reduction of the average valence of TM cations during the long-term cycling.[55] By comparison, the NCM with PAM-QSE barely exhibits peak shifts and intensity variations. The EELS results suggest the reduction of highly reactive Ni^{4+} toward Ni^{2+} and the structural robustness of NCM cathode with PAM-QSE, strongly confirming the superiority of antioxidative CEI layer that contains rich polyamide molecules.

In summary, in pursuit of implementing high voltage lithium metal batteries with high safety and superior cycling performance, we constructed a flame-retardant polyamide-based quasi-solid electrolyte (PAM-QSE) with dual-reinforced interface stability. During cycling, on the Li metal anode, the participation of PAM-QSE in the composition of SEI layer structure enables abundant inorganic Li_3N with high ion conductivity and lithiophilic $N-(C)_3$ organic groups to contribute the fast transport and homogeneous deposition of Li^+. On the Ni-rich NCM cathode, the CEI layer comprises high antioxidant components derived from polyamide molecules, which is conducive to protect the active cathode materials from electrolyte erosion and irreversible structural degradation. These results not only indicate that PAM-QSE represents a promising electrolyte for Ni-rich NCM/Li metal batteries but also provide new perspectives for stabilizing electrodes/electrolyte interphases through manipulation of interface chemistry.

■ ASSOCIATED CONTENT

Supporting Information

The Supporting Information is available free of charge at https://pubs.acs.org/doi/10.1021/acsenergylett.1c00265.

Experimental methods, additional morphological and electrochemical characterizations, and more discussion (PDF)

■ AUTHOR INFORMATION

Corresponding Author

Weifeng Wei − *State Key Laboratory of Powder Metallurgy, Central South University, Changsha, Hunan 410083, People's Republic of China;* orcid.org/0000-0002-3088-6549; Email: weifengwei@csu.edu.cn

Authors

Minjian Chen − *State Key Laboratory of Powder Metallurgy, Central South University, Changsha, Hunan 410083, People's Republic of China*

Cheng Ma − *State Key Laboratory of Powder Metallurgy, Central South University, Changsha, Hunan 410083, People's Republic of China*

Zhengping Ding − *International Center for Quantum Materials, and Electron Microscopy Laboratory, School of Physics, Peking University, Beijing 100871, People's Republic of China; Collaborative Innovation Center of Quantum Matter, Beijing 100871, People's Republic of China;* orcid.org/0000-0001-5275-5905

Liangjun Zhou − *State Key Laboratory of Powder Metallurgy, Central South University, Changsha, Hunan 410083, People's Republic of China*

Libao Chen − *State Key Laboratory of Powder Metallurgy, Central South University, Changsha, Hunan 410083, People's Republic of China*

Peng Gao − *International Center for Quantum Materials, and Electron Microscopy Laboratory, School of Physics, Peking University, Beijing 100871, People's Republic of China; Collaborative Innovation Center of Quantum Matter, Beijing 100871, People's Republic of China;* orcid.org/0000-0003-0860-5525

Complete contact information is available at: https://pubs.acs.org/10.1021/acsenergylett.1c00265

Author Contributions

‖M.C. and C.M. contributed equally to this work.

Notes

The authors declare no competing financial interest.

■ ACKNOWLEDGMENTS

The authors acknowledge financial support from the National Natural Science Foundation of China (Grants 51304248, 11874199, 51971250, 51672007, and 11974023), the National Key Research and Development Program of China (Grant 2018YFB010400), SAFEA: High-End Foreign Experts Project (Grant B06020), the National Basic Research Program of China (Grant 2015CB654901), the State Key Laboratory of Powder Metallurgy at Central South University, and the Shenzhen GuoTuo Technology Co., Ltd.

■ REFERENCES

(1) Sun, Y. K.; Myung, S. T.; Park, B. C.; Prakash, J.; Belharouak, I.; Amine, K. High-energy cathode material for long-life and safe lithium batteries. *Nat. Mater.* **2009**, *8* (4), 320–4.

(2) Etacheri, V.; Marom, R.; Elazari, R.; Salitra, G.; Aurbach, D. Challenges in the development of advanced Li-ion batteries: a review. *Energy Environ. Sci.* **2011**, *4* (9), 3243.

(3) Manthiram, A. A reflection on lithium-ion battery cathode chemistry. *Nat. Commun.* **2020**, *11* (1), 1550.

(4) Hu, M.; Pang, X.; Zhou, Z. Recent progress in high-voltage lithium ion batteries. *J. Power Sources* **2013**, *237*, 229–242.

(5) Zhang, S.; Ma, J.; Hu, Z.; Cui, G.; Chen, L. Identifying and Addressing Critical Challenges of High-Voltage Layered Ternary Oxide Cathode Materials. *Chem. Mater.* **2019**, *31* (16), 6033−6065.
(6) Liu, W.; Oh, P.; Liu, X.; Lee, M. J.; Cho, W.; Chae, S.; Kim, Y.; Cho, J. Nickel-rich layered lithium transition-metal oxide for high-energy lithium-ion batteries. *Angew. Chem., Int. Ed.* **2015**, *54*, 4440.
(7) Kim, J.; Lee, H.; Cha, H.; Yoon, M.; Park, M.; Cho, J. Prospect and Reality of Ni-Rich Cathode for Commercialization. *Adv. Energy Mater.* **2018**, *8* (6), 1702028.
(8) Lin, D.; Liu, Y.; Cui, Y. Reviving the lithium metal anode for high-energy batteries. *Nat. Nanotechnol.* **2017**, *12* (3), 194−206.
(9) Wu, F.; Yuan, Y.-X.; Cheng, X.-B.; Bai, Y.; Li, Y.; Wu, C.; Zhang, Q. Perspectives for restraining harsh lithium dendrite growth: Towards robust lithium metal anodes. *Energy Storage Mater.* **2018**, *15*, 148−170.
(10) Li, Z.; Zhang, H.; Sun, X.; Yang, Y. Mitigating Interfacial Instability in Polymer Electrolyte-Based Solid-State Lithium Metal Batteries with 4 V Cathodes. *ACS Energy Letters* **2020**, *5* (10), 3244−3253.
(11) Kasnatscheew, J.; Streipert, B.; Roser, S.; Wagner, R.; Cekic Laskovic, I.; Winter, M. Determining oxidative stability of battery electrolytes: validity of common electrochemical stability window (ESW) data and alternative strategies. *Phys. Chem. Chem. Phys.* **2017**, *19* (24), 16078−16086.
(12) Streipert, B.; Stolz, L.; Homann, G.; Janssen, P.; Cekic-Laskovic, I.; Winter, M.; Kasnatscheew, J. Conventional Electrolyte and Inactive Electrode Materials in Lithium-Ion Batteries: Determining Cumulative Impact of Oxidative Decomposition at High Voltage. *ChemSusChem* **2020**, *13* (19), 5301−5307.
(13) Jung, R.; Metzger, M.; Maglia, F.; Stinner, C.; Gasteiger, H. A. Chemical versus Electrochemical Electrolyte Oxidation on NMC111, NMC622, NMC811, LNMO, and Conductive Carbon. *J. Phys. Chem. Lett.* **2017**, *8* (19), 4820−4825.
(14) Xu, K. Nonaqueous Liquid Electrolytes for Lithium-Based Rechargeable Batteries. *Chem. Rev.* **2004**, *104*, 4303.
(15) Freiberg, A. T. S.; Sicklinger, J.; Solchenbach, S.; Gasteiger, H. A. Li_2CO_3 decomposition in Li-ion batteries induced by the electrochemical oxidation of the electrolyte and of electrolyte impurities. *Electrochim. Acta* **2020**, *346*, 136271.
(16) Kasnatscheew, J.; Evertz, M.; Streipert, B.; Wagner, R.; Nowak, S.; Cekic Laskovic, I.; Winter, M. Changing Established Belief on Capacity Fade Mechanisms: Thorough Investigation of $LiNi_{1/3}Co_{1/3}Mn_{1/3}O_2$ (NCM111) under High Voltage Conditions. *J. Phys. Chem. C* **2017**, *121* (3), 1521−1529.
(17) Homann, G.; Stolz, L.; Neuhaus, K.; Winter, M.; Kasnatscheew, J. Effective Optimization of High Voltage Solid-State Lithium Batteries by Using Poly(ethylene oxide)-Based Polymer Electrolyte with Semi-Interpenetrating Network. *Adv. Funct. Mater.* **2020**, *30* (46), 2006289.
(18) Yang, C.; Fu, K.; Zhang, Y.; Hitz, E.; Hu, L. Protected Lithium-Metal Anodes in Batteries: From Liquid to Solid. *Adv. Mater.* **2017**, *29* (36), 1701169.
(19) Han, F.; Westover, A. S.; Yue, J.; Fan, X.; Wang, F.; Chi, M.; Leonard, D. N.; Dudney, N. J.; Wang, H.; Wang, C. High electronic conductivity as the origin of lithium dendrite formation within solid electrolytes. *Nat. Energy* **2019**, *4* (3), 187−196.
(20) Yu, X.; Manthiram, A. Electrode−electrolyte interfaces in lithium-based batteries. *Energy Environ. Sci.* **2018**, *11* (3), 527−543.
(21) Kaboli, S.; Demers, H.; Paolella, A.; Darwiche, A.; Dontigny, M.; Clement, D.; Guerfi, A.; Trudeau, M. L.; Goodenough, J. B.; Zaghib, K. Behavior of Solid Electrolyte in Li-Polymer Battery with NMC Cathode via in-Situ Scanning Electron Microscopy. *Nano Lett.* **2020**, *20* (3), 1607−1613.
(22) Wang, H.; Huang, W.; Yu, Z.; Huang, W.; Xu, R.; Zhang, Z.; Bao, Z.; Cui, Y. Efficient Lithium Metal Cycling over a Wide Range of Pressures from an Anion-Derived Solid-Electrolyte Interphase Framework. *ACS Energy Letters* **2021**, *6*, 816−825.
(23) Yang, L.; Yang, K.; Zheng, J.; Xu, K.; Amine, K.; Pan, F. Harnessing the surface structure to enable high-performance cathode materials for lithium-ion batteries. *Chem. Soc. Rev.* **2020**, *49* (14), 4667−4680.
(24) Wang, Y.; Zhang, Q.; Xue, Z. C.; Yang, L.; Wang, J.; Meng, F.; Li, Q.; Pan, H.; Zhang, J. N.; Jiang, Z.; Yang, W.; Yu, X.; Gu, L.; Li, H. An In Situ Formed Surface Coating Layer Enabling $LiCoO_2$ with Stable 4.6 V High-Voltage Cycle Performances. *Adv. Energy Mater.* **2020**, *10* (28), 2001413.
(25) Xu, G.-L.; Liu, Q.; Lau, K. K. S.; Liu, Y.; Liu, X.; Gao, H.; Zhou, X.; Zhuang, M.; Ren, Y.; Li, J.; Shao, M.; Ouyang, M.; Pan, F.; Chen, Z.; Amine, K.; Chen, G. Building ultraconformal protective layers on both secondary and primary particles of layered lithium transition metal oxide cathodes. *Nat. Energy* **2019**, *4* (6), 484−494.
(26) Shen, Y.; Zhang, Y.; Han, S.; Wang, J.; Peng, Z.; Chen, L. Unlocking the Energy Capabilities of Lithium Metal Electrode with Solid-State Electrolytes. *Joule* **2018**, *2* (9), 1674−1689.
(27) Hao, X.; Zhao, Q.; Su, S.; Zhang, S.; Ma, J.; Shen, L.; Yu, Q.; Zhao, L.; Liu, Y.; Kang, F.; He, Y. B. Constructing Multifunctional Interphase between $Li_{1.4}Al_{0.4}Ti_{1.6}(PO_4)_3$ and Li Metal by Magnetron Sputtering for Highly Stable Solid-State Lithium Metal Batteries. *Adv. Energy Mater.* **2019**, *9* (34), 1901604.
(28) Han, Y.; Heng, S.; Wang, Y.; Qu, Q.; Zheng, H. Anchoring Interfacial Nickel Cations on Single-Crystal $LiNi_{0.8}Co_{0.1}Mn_{0.1}O_2$ Cathode Surface via Controllable Electron Transfer. *ACS Energy Letters* **2020**, *5* (7), 2421−2433.
(29) Li, X.; Liu, J.; Banis, M. N.; Lushington, A.; Li, R.; Cai, M.; Sun, X. Atomic layer deposition of solid-state electrolyte coated cathode materials with superior high-voltage cycling behavior for lithium ion battery application. *Energy Environ. Sci.* **2014**, *7* (2), 768−778.
(30) Lang, J.; Long, Y.; Qu, J.; Luo, X.; Wei, H.; Huang, K.; Zhang, H.; Qi, L.; Zhang, Q.; Li, Z.; Wu, H. One-pot solution coating of high quality LiF layer to stabilize Li metal anode. *Energy Storage Mater.* **2019**, *16*, 85−90.
(31) Sun, H. H.; Ryu, H.-H.; Kim, U.-H.; Weeks, J. A.; Heller, A.; Sun, Y.-K.; Mullins, C. B. Beyond Doping and Coating: Prospective Strategies for Stable High-Capacity Layered Ni-Rich Cathodes. *ACS Energy Letters* **2020**, *5* (4), 1136−1146.
(32) Lee, S. H.; Hwang, J. Y.; Park, S. J.; Park, G. T.; Sun, Y. K. Adiponitrile ($C_6H_8N_2$): A New Bi-Functional Additive for High-Performance Li-Metal Batteries. *Adv. Funct. Mater.* **2019**, *29* (30), 1902496.
(33) Kim, K.; Hwang, D.; Kim, S.; Park, S. O.; Cha, H.; Lee, Y. S.; Cho, J.; Kwak, S. K.; Choi, N. S. Cyclic Aminosilane-Based Additive Ensuring Stable Electrode−Electrolyte Interfaces in Li-Ion Batteries. *Adv. Energy Mater.* **2020**, *10* (15), 2000012.
(34) Li, Z. F.; Lin, X. Y.; Zhou, H. B.; Xing, L. D.; Lan, G. Y.; Zhang, W. G.; Chen, J. W.; Liu, M. Z.; Huang, Q. M.; Li, W. S. Stabilizing the interphasial layer of Ni-rich cathode and graphite anode for lithium ion battery with multifunctional additive. *J. Power Sources* **2020**, *467*, 228343.
(35) Gao, H.; Maglia, F.; Lamp, P.; Amine, K.; Chen, Z. Mechanistic Study of Electrolyte Additives to Stabilize High-Voltage Cathode-Electrolyte Interface in Lithium-Ion Batteries. *ACS Appl. Mater. Interfaces* **2017**, *9* (51), 44542−44549.
(36) Liang, J. Y.; Zhang, X. D.; Zeng, X. X.; Yan, M.; Yin, Y. X.; Xin, S.; Wang, W. P.; Wu, X. W.; Shi, J. L.; Wan, L. J.; Guo, Y. G. Enabling a Durable Electrochemical Interface via an Artificial Amorphous Cathode Electrolyte Interphase for Hybrid Solid/Liquid Lithium-Metal Batteries. *Angew. Chem., Int. Ed.* **2020**, *59* (16), 6585−6589.
(37) Sun, H.; Zhu, G.; Zhu, Y.; Lin, M. C.; Chen, H.; Li, Y. Y.; Hung, W. H.; Zhou, B.; Wang, X.; Bai, Y.; Gu, M.; Huang, C. L.; Tai, H. C.; Xu, X.; Angell, M.; Shyue, J. J.; Dai, H. High-Safety and High-Energy-Density Lithium Metal Batteries in a Novel Ionic-Liquid Electrolyte. *Adv. Mater.* **2020**, *32* (26), e2001741.
(38) Xiao, Y.; Wang, Y.; Bo, S.-H.; Kim, J. C.; Miara, L. J.; Ceder, G. Understanding interface stability in solid-state batteries. *Nat. Rev. Mater.* **2020**, *5* (2), 105−126.
(39) Liao, C. Electrolytes and additives for batteries Part I: fundamentals and insights on cathode degradation mechanisms. *eTransportation* **2020**, *5*, 100068.

(40) Xiong, B.-Q.; Zhou, X.; Xu, G.-L.; Liu, X.; Hu, Y.; Liu, Y.; Zhu, L.; Shi, C.-G.; Hong, Y.-H.; Wan, S.-C.; Sun, C.-J.; Chen, S.; Huang, L.; Sun, S.-G.; Amine, K.; Ke, F.-S. In Situ Construction of an Ultrarobust and Lithiophilic Li-Enriched Li−N Nanoshield for High-Performance Ge-Based Anode Materials. *ACS Energy Letters* **2020**, *5* (11), 3490−3497.
(41) Liu, Y.; Lin, D.; Yuen, P. Y.; Liu, K.; Xie, J.; Dauskardt, R. H.; Cui, Y. An Artificial Solid Electrolyte Interphase with High Li-Ion Conductivity, Mechanical Strength, and Flexibility for Stable Lithium Metal Anodes. *Adv. Mater.* **2017**, *29* (10), 1605531.
(42) Xu, H.; Li, Y.; Zhou, A.; Wu, N.; Xin, S.; Li, Z.; Goodenough, J. B. Li_3N-Modified Garnet Electrolyte for All-Solid-State Lithium Metal Batteries Operated at 40 degrees C. *Nano Lett.* **2018**, *18* (11), 7414−7418.
(43) Zhang, W.; Zhang, S.; Fan, L.; Gao, L.; Kong, X.; Li, S.; Li, J.; Hong, X.; Lu, Y. Tuning the LUMO Energy of an Organic Interphase to Stabilize Lithium Metal Batteries. *ACS Energy Letters* **2019**, *4* (3), 644−650.
(44) Li, Y.; An, Y.; Tian, Y.; Fei, H.; Xiong, S.; Qian, Y.; Feng, J. Stable and Safe Lithium Metal Batteries with Ni-Rich Cathodes Enabled by a High Efficiency Flame Retardant Additive. *J. Electrochem. Soc.* **2019**, *166* (13), A2736−A2740.
(45) Liu, J.; Song, X.; Zhou, L.; Wang, S.; Song, W.; Liu, W.; Long, H.; Zhou, L.; Wu, H.; Feng, C.; Guo, Z. Fluorinated phosphazene derivative − A promising electrolyte additive for high voltage lithium ion batteries: From electrochemical performance to corrosion mechanism. *Nano Energy* **2018**, *46*, 404−414.
(46) Gupta, H.; Shalu, S.; Balo, L.; Singh, V. K.; Chaurasia, S. K.; Singh, R. K. Effect of phosphonium based ionic liquid on structural, electrochemical and thermal behaviour of polymer poly(ethylene oxide) containing salt lithium bis(trifluoromethylsulfonyl)imide. *RSC Adv.* **2016**, *6* (91), 87878−87887.
(47) Gupta, H.; Kataria, S.; Balo, L.; Singh, V. K.; Singh, S. K.; Tripathi, A. K.; Verma, Y. L.; Singh, R. K. Electrochemical study of Ionic Liquid based polymer electrolyte with graphene oxide coated LiFePO4 cathode for Li battery. *Solid State Ionics* **2018**, *320*, 186−192.
(48) Singh, S. K.; Dutta, D.; Singh, R. K. Enhanced structural and cycling stability of Li_2CuO_2-coated $LiNi_{0.33}Mn_{0.33}Co_{0.33}O_2$ cathode with flexible ionic liquid-based gel polymer electrolyte for lithium polymer batteries. *Electrochim. Acta* **2020**, *343*, 136122.
(49) Xian, F.; Li, J.; Hu, Z.; Zhou, Q.; Wang, C.; Lu, C.; Zhang, Z.; Dong, S.; Mou, C.; Cui, G. Investigation of the cathodic interfacial stability of a nitrile electrolyte and its performance with a high-voltage $LiCoO_2$ cathode. *Chem. Commun.* **2020**, *56* (37), 4998−5001.
(50) Wang, Q.; Yao, Z.; Zhao, C.; Verhallen, T.; Tabor, D. P.; Liu, M.; Ooms, F.; Kang, F.; Aspuru-Guzik, A.; Hu, Y. S.; Wagemaker, M.; Li, B. Interface chemistry of an amide electrolyte for highly reversible lithium metal batteries. *Nat. Commun.* **2020**, *11* (1), 4188.
(51) Ye, S.; Wang, L.; Liu, F.; Shi, P.; Wang, H.; Wu, X.; Yu, Y. g-C_3N_4 Derivative Artificial Organic/Inorganic Composite Solid Electrolyte Interphase Layer for Stable Lithium Metal Anode. *Adv. Energy Mater.* **2020**, *10* (44), 2002647.
(52) Lee, D.; Sun, S.; Kwon, J.; Park, H.; Jang, M.; Park, E.; Son, B.; Jung, Y.; Song, T.; Paik, U. Copper Nitride Nanowires Printed Li with Stable Cycling for Li Metal Batteries in Carbonate Electrolytes. *Adv. Mater.* **2020**, *32* (7), e1905573.
(53) Eshetu, G. G.; Judez, X.; Li, C.; Bondarchuk, O.; Rodriguez-Martinez, L. M.; Zhang, H.; Armand, M. Lithium Azide as an Electrolyte Additive for All-Solid-State Lithium-Sulfur Batteries. *Angew. Chem., Int. Ed.* **2017**, *56* (48), 15368−15372.
(54) Ruan, Y.; Song, X.; Fu, Y.; Song, C.; Battaglia, V. Structural evolution and capacity degradation mechanism of $LiNi_{0.6}Mn_{0.2}Co_{0.2}O_2$ cathode materials. *J. Power Sources* **2018**, *400*, 539−548.
(55) Li, W.; Liu, X.; Xie, Q.; You, Y.; Chi, M.; Manthiram, A. Long-Term Cyclability of NCM-811 at High Voltages in Lithium-Ion Batteries: an In-Depth Diagnostic Study. *Chem. Mater.* **2020**, *32* (18), 7796−7804.

https://dx.doi.org/10.1021/acsenergylett.1c00265
ACS Energy Lett. 2021, 6, 1280−1289